Journal of Applied Polymer Science

Synthesis and characterization of sulfonated fluorinated block copolymer membranes with different esterified initiators for DMFC applications

Edward M. A. Guerrero-Gutiérrez, Maritza Pérez-Pérez, David Suleiman
Chemical Engineering Department, University of Puerto Rico, Mayagüez, Puerto Rico 00681-9000
Correspondence to: D. Suleiman (E-mail: David.Suleiman@upr.edu)

ABSTRACT: This investigation studied the synthesis of ionic membranes composed of a sulfonated poly(styrene-isobutylene-styrene) with novel fluoroblock copolymers. These fluoroblock copolymers were synthesized using three different initiators by Atom Transfer Radical Polymerization (ATRP); two fluoroinitiators were obtained from the esterification of 2-(perfluoroalkyl) ethanol or octafluoro 4-4′-biphenol. The third initiator evaluated was 1-bromoethyl benzene. The resulting block copolymers were characterized using several techniques: Gel Permeation Chromatography, Nuclear Magnetic Resonance, Fourier Transform Infrared Spectroscopy, Ultraviolet Spectroscopy, Thermogravimetric Analysis, and Differential Scanning Calorimetry. Transport properties (e.g., proton conductivity and methanol permeability) were measured to evaluate their performance for direct methanol fuel cell (DMFC). The choice of ATRP initiator was found to have a profound impact on the thermal stability of the different homopolymers and block copolymers studied. In addition, the chemical nature and symmetry of the initiators can lead to different chemical and electronic transitions, which influence the performance of these ionic membranes in applications such as proton exchange membranes for DMFC applications. © 2015 Wiley Periodicals, Inc. J. Appl. Polym. Sci. **2015**, *132*, 42046.

KEYWORDS: batteries and fuel cells; conducting polymers; degradation; membranes; nanostructured polymers

Received 14 November 2014; accepted 23 January 2015
DOI: 10.1002/app.42046

INTRODUCTION

Fluorinated polymers are used in numerous and diverse functional materials because they possess high thermal stability, enhanced chemical resistance, and low surface energy compared to their nonfluorinated analogs.[1] Applications for these polymers include: proton conducting materials,[2] stabilizers for emulsion polymerization,[3] additives in oil recovery and water treatment,[4] surfactants,[5] lubricants,[6] and ion conducting materials.[7] Proton exchange membranes (PEM's) for direct methanol fuel cells (DMFC) is another application where sulfonated fluoropolymers (e.g., Nafion®) are used, because they possess high proton conductivity and excellent thermal, mechanical and barrier properties.[8–14] Our group has worked with different PEM's for DMFC that explored different chemical functionalities[15,16] and processing approaches to influence morphology.[17,18] These studies have demonstrated the sensitivity of the transport properties to the resulting nanostructure and the electronic configuration inside the resulting ionic nanochannels.

Controlled radical polymerization (CRP) allows for the synthesis of advanced well-defined fluoropolymers with specific structures and low polydispersity.[19] Morphology and the chemical structure contribute to the mechanical, physical, thermal and chemical properties in polymeric materials.[20] CRP methods generally rely on a reversible activation-deactivation process between dormant and active polymer chains, and as the double bond of monomers containing fluorine is additionally activated by the electron withdrawing group, this sometimes leads to considerably higher rates of polymerization.[21] Atom transfer radical polymerization (ATRP) is a CRP technique that uses an alkyl halide like initiator, a transition metal in the lower oxidation state, and a ligand to synthesize different fluoropolymers. Initiators for ATRP must have a halogen (Br or Cl) and a functional group that can stabilize the formed radical.[22] Homopolymer containing poly(2,3,4,5,6-pentafluorostyrene),[23] diblock copolymers containing 4-fluorostyrene and methyl acrylate,[24] and phosphonated fluoropolymers[25,26] were prepared by ATRP.

Chemical modification on terminal groups of fluoroalcohols[27,28] and polymers like poly(ethylene glycol) (PEG)[29] have been synthesized with the aim to obtain novel ATRP initiators. A limited number of studies have evaluated the effect of different initiators on the thermal stability and resulting properties of the polymers. Even less investigations have focused on the thermal

stability and transport properties (for DMFC applications), of fluoroblock copolymers made with different esterified initiators. Howell *et al.*[30] evaluated the impact of the initiator's characteristics on the thermal stability of vinylidene chloride copolymers. In their study, the polymer was synthesized by a radical suspension technique using four different initiators with similar decomposition temperature. The results showed that the changes in the thermal stability of the copolymers were probably induced by the introduction either via end-group effects, or by attack of residual initiator fragments on the finished polymer during isolation and residual monomer stripping.[30] Jankova and Hvilsted[31] modified chemically dipentaerythritol using an esterification reaction to obtain an ATRP initiator. A hexa-arm star diblock copolymer of styrene and 2,3,4,5,6-pentafluorostyrene was synthesized. The thermal degradation for this polymer presented lower temperature degradation, suggesting that a thermal degradation involved scission of the ester linkages in the polymer.[31]

Esterified initiators seem to have a strong influence on the thermal stability of block copolymers. Therefore, the first goal of this investigation was to evaluate the effect of different esterified initiators on the thermal properties of four novel fluoro diblock copolymers and their homopolymers synthesized by ATRP. The block copolymers were based on polystyrene (PS) and 2,2,3,4,4,4-hexafluorobutyl methacrylate (HFBMA). The initiators studied were obtained from the esterification of 2-(perfluoroalkyl) ethanol (Zonyl®) and octafluoro 4-4′-biphenol (octo). The third initiator studied was the conventional 1-bromo ethyl benzene (EtlB) for ATRP reactions. Since this communication compared different homopolymers and diblock copolymers, the nomenclature for the different polymers studied starts with the initiator, followed by the polymer or block copolymer studied. For example, Zonyl®-PS-b-PHFBMA represents the block copolymer poly(styrene) with poly(2,2,3,4,4,4-hexafluorobutyl methacrylate) initiated with esterified 2-(perfluoroalkyl) ethanol.

Esterified Zonyl® was evaluated based on a previous study,[27] where well-defined methacrylic copolymers were synthesized, but lacked the evaluation of the thermal stability and the polymerization of other blocks with different chemical structure, like styrene. In addition, it lacked the connection with transport properties for DMFC applications. The resulting homo and diblock copolymers were chemically characterized using Nuclear Magnetic Resonance (NMR) and Fourier Transform Infrared Spectroscopy (FTIR). Thermal properties were analyzed by TGA. Molecular weights were obtained by Gel Permeation Chromatography (GPC) and the electronic transitions were analyzed with ultraviolet (UV) spectroscopy. Furthermore, the transport properties of ionic blend membranes composed of a sulfonated poly(styrene-b-isobutylene-b-styrene) (SIBS SO_3H) with novel fluoropolymer based on poly(styrene) were investigated; therefore, the second goal of this investigation was to evaluate the influence of the initiator on the resulting transport properties of these membranes for DMFC applications.

EXPERIMENTAL

Materials

SIBS was purchased from Kaneka® (30 wt. % PS and M_n∼65,000 g/mole). Sulfuric acid (Sigma Aldrich, 95–98%), acetic anhydride (Aldrich Chemical, 99+%), hexyl alcohol (Acros Organics, 98%, extra pure), methanol (Fisher Scientific, 99.9%), toluene American Chemical Society (ACS) reagent (99%) and dichloromethane were acquired from Fisher Scientific. Zonyl® BA-L Fluorotelomer intermediate (70 wt %) Mn∼443 was acquired from Sigma-Aldrich. Octafluoro-4-4′-biphenol was acquired from Tokyo Chemical Industry CO. Toluene ACS reagent (99%) and dichloromethane (99.9%) were acquired from Fisher Scientific. Other chemicals used include: 1-bromo ethyl benzene (Acros-Organics, 97%), triethylamine, (Acros-Organics, 99%), 4-dimethylamino pyridine, (Acros Organics, 99%), 2-chloropropionyl chloride, (Acros-Organics, 95%), 2, 2′-dipyridyl – Bipy - (Acros Organics, extra pure, 99%), calcium hydride -CaH_2- (Acros-Organics, 93%), and copper (I) chloride (Acros-Organics, 99%). All chemicals were used as received. The monomers used included: HFBMA (Alfa Aesar 96% inhibited with monomethyl ether hydroquinone –MEHQ-) and styrene (Across Organics, 99% inhibited with 4-tert-butyl catechol). Both monomers were passed through an inhibitor remover (disposable column from Sigma-Aldrich). After this process both monomers

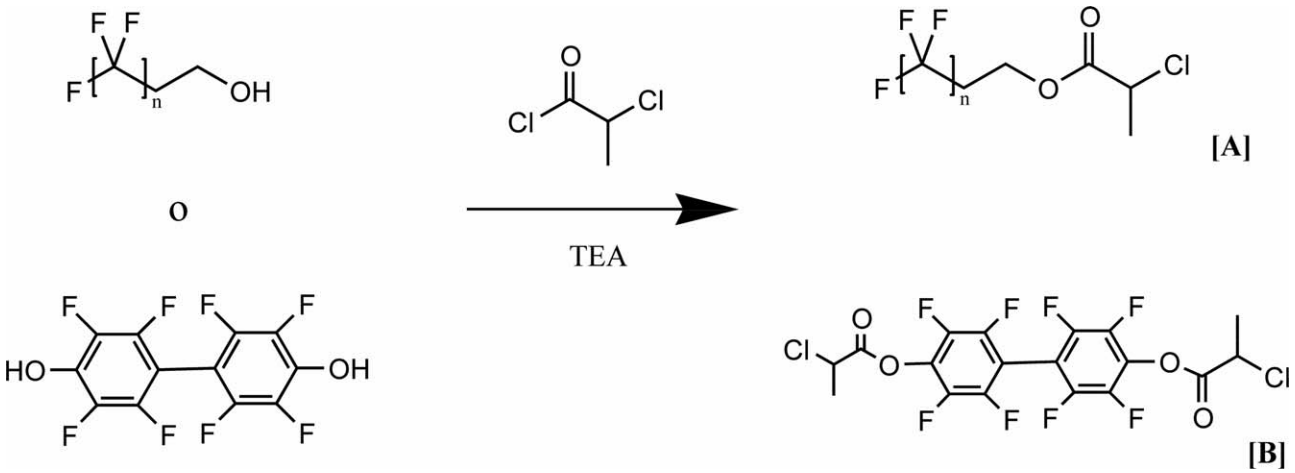

Scheme 1. Esterification reaction for (perfluoroalkyl)ethanol (Zonyl®) (A) and octafluoro 4-4′ biphenol (B).

and the solvent were stored over CaH_2 and then vacuum-distilled before polymerization. Nafion® 117 was obtained from Ion Power.

Esterification of 2-Perfluoroalkyl Ethanol and Octafluoro-4-4′-Biphenol

2-(perfluoroalkyl) ethanol (Zonyl®) and, octafluoro 4-4′-biphenol were chemically modified using an esterification reaction, with the purpose of obtaining esterified compounds capable of initiating a polymeric reaction in an ATRP process. Scheme 1 shows the esterification pathway to synthesize esterified (Zonyl®) and esterified octafluoro 4-4′-biphenol initiators. Zonyl® and 4-dimethylamino pyridine were dissolved in toluene at 60°C. Triethylamine and 2-chloropropionyl chloride were added and the reaction was stopped after 24 h.[27] Toluene was removed by rotary evaporation. The obtained product was dissolved using dichloromethane and washed with a saturated $NaHCO_3$ solution, 1*M* HCl, and distilled water. The solvents were removed by rotary evaporation.

ATRP Homopolymerization Using Esterified Initiators and 1-Bromo Ethyl Benzene

In a characteristic homopolymerization by ATRP, a Schlenk tube was charged with the initiator (e.g., esterified Zonyl® or 1-bromo ethyl benzene), copper chloride (CuCl), and the 2, 2′-dipyridyl (bipy). The molar ratio of initiator:CuCl:bipy was kept 1:1:2.[32] The monomer was added, and the system was degassed three times by freezing and thawing; then heating to the desired temperature (110°C) under a nitrogen atmosphere. On completion of the experiment, the polymerization mixture was diluted with THF. The solution was filtered (to remove the catalyst) and then precipitated in methanol, where the polymer appeared as a fluffy white material that was recovered after vacuum drying.

ATRP Copolymerization

In a typical block copolymerization by ATRP, a Schlenk tube was charged with the macroinitiator, copper chloride (CuCl) and the 2, 2′-dipyridyl. The molar ratio of initiator:CuCl:bipy was kept 1:1:2.[32] The system was degassed three times minimum by freezing and thawing. After three freeze-thaw cycles, the mixture was heated (110°C) for 24 h under a nitrogen atmosphere. The block copolymer solution was filtered and then precipitated in methanol. All the polymerization reactions for the homo and diblock copolymers are presented in Scheme 2.

Characterization of Homo, Di-Block Copolymers and Polymer Blends

FTIR was used to identify the chemical nature of the polymers and the membranes analyzing the vibrational band of the functional groups. An attenuated total reflectance (ATR) cell was used with an FTIR (Varian 800 FTIR) to characterize the homo,

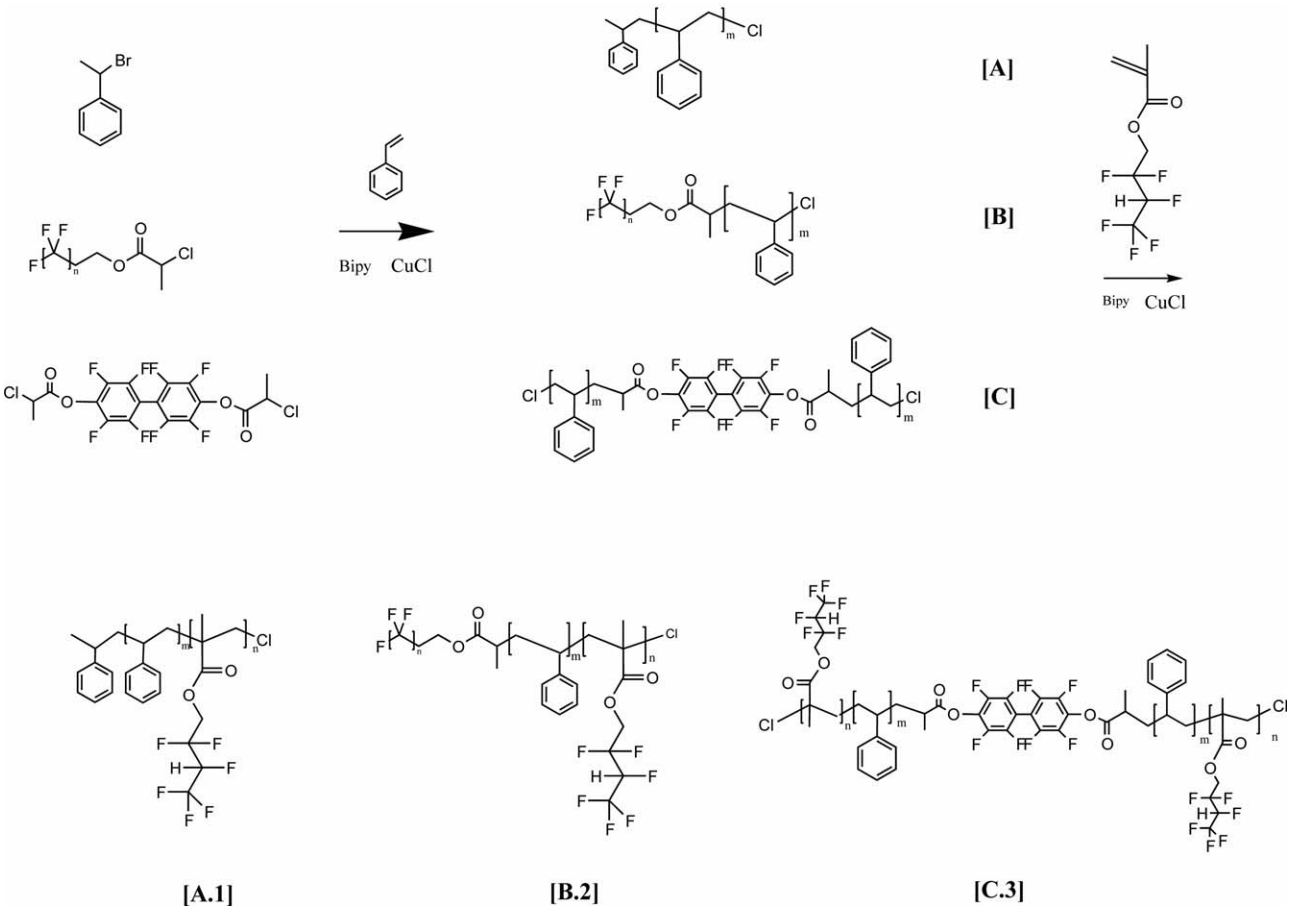

Scheme 2. Polymerization reaction for EtlB-PS-b-PHFBMA (A.1), Zonyl®-PS-b-PHFBMA (B.2), and octo-PS-b-PHFBMA (C.3).

diblock copolymers and the polymeric membranes. The sample was clamped on the ATR cell and all infrared spectra were collected using 64 scans, 4 cm^{-1} resolution and a range of 600–4000 cm^{-1}. The homopolymers and the block copolymers were characterized by ^1H NMR, using a NMR Bruker 500 MHz spectrometer with chloroform-d as a solvent.

A UV-VIS spectrophotomer equipment (Shimatzu UV-2401 P) was used to characterize the homo and diblock copolymers. The sample was placed in a quartz ultramicrocell for measurement. UV spectra were collected using 1 nm intervals and a range of 200–600 nm; THF was used as the solvent.

GPC was performed on a Waters GPC system equipped with a mixed column (PLgel 5 μm MIXED-C, Varian) and a differential refractometer (BI-DNDC, Brookhaven Instruments). THF HPLC solvent was used as the mobile phase with a flow rate of 0.5 mL/min. Molecular weight distributions were obtained with reference to PS standards (Varian).

The thermal degradation behavior for each homo, diblock copolymer and polymer blends were determined using TGA. A Mettler Toledo 851e instrument was used for this purpose. In each experiment, polymer samples weighting approximately 5–10 mg were used. Degradation temperatures were determined after heating the polymer samples to 800°C at 10°C/min under a nitrogen atmosphere.

Thermo physical properties were determined using Differential Scanning Calorimetry (DSC). A Texas Instrument DSC Q2000 unit was used for this purpose. In each experiment, polymer samples weighting approximately 5–10 mg were used. Thermal transitions for each membrane were determined after heating the polymer samples from −80°C to 350°C at 10°C/min under a nitrogen atmosphere.

Blend Preparation

SIBS was sulfonated using acetyl sulfate as the sulfonating agent. The sulfonation process is described in more detail elsewhere.[16] Sulfonated SIBS (SIBS SO_3H) was used to prepare polymer blends with the fluoropolymers. The preparation of physical blends consisted of mixing SIBS SO_3H (86wt %) and unsulfonated fluoropolymer (14 wt %) [EtlB-PS, Zonyl®-PS or Octo-PS]. SIBS SO_3H and the fluoropolymer were dissolved in a solution (85/15) (v/v) of toluene and hexyl alcohol with a polymer concentration of 5 wt %. SIBS SO_3H/fluoropolymer membranes were solvent casted in Teflon® Petri dishes for 96 h at room temperature as the solvent evaporated; then dried at 60°C for 24 h to remove the residual solvent.

Methanol Liquid-Phase Permeability

The methanol liquid-phase permeability was measured using a side-by-side glass diffusion cell discussed in detail elsewhere.[17] One side contained the permeant (e.g., methanol) in a 2*M* methanol-water solution, while the other side only contained deionized water. The concentration of the compound that permeated through the membrane was determined using a gas chromatograph (GC) equipped with a thermal conductivity detector (Shimadzu GC-8). First a calibration curve was created, then measurements were determined after different times. The liquid permeability was obtained from the continuity equation for diffusion in plane geometry[33] eq. (1):

$$C_B(t) = \frac{PC_A A}{V_b L}\left(t - \frac{L^2}{6D}\right) \quad (1)$$

where, C_A (mole/cm^3) is the methanol concentration (permeant), C_B (mole/cm^3) is the concentration of the compound that permeated thought the membrane after different times, L is the membrane thickness, V_b the volume of the receptor compartment (cm^3), A the diffusional cross-sectional area of the membrane (0.632 cm^2), and P the permeability (cm^2/s). The permeability (P) was determined from the slope of the concentration $C_B(t)$ versus time.[34]

Proton Conductivity

The proton conductivity (σ) of each membrane was carried out on a Fuel Cell Test System (850e Multi Range) equipped with an 885 Fuel Cell Potentiostat from Scribner Associate Incorporated. The range of frequency and the AC amplitude used were from 0.1 to 100,000 Hz and 0.1 Amps, respectively at 40°C and 100% relative humidity. The membranes were first immersed in an excess of deionized water at 25°C before the experimentation during 24 h. The proton conductivity was calculated from the impedance data, using the following relation eq. (2):[35]

$$\sigma = \frac{L}{R_\Omega A} \quad (2)$$

where L and A (cm^2) are the membrane thickness and area, respectively. R_Ω was obtained from the low intersect of the high frequency semicircle (Nyquist plot) on the complex impedance plane with the real component of the impedance axis (Re(z)).

Water Uptake

Water uptake in the membranes was measured immersing each membrane in an excess of deionized water at 25°C. The weight of the sample (initially dried at 60°C for 24 h in an oven) was originally recorded, as well as the weight of the membrane after immersion in water. The weights of the wet membrane were measured after different time intervals until swelling equilibrium was reached. Each reported result represents the average of at least three repetitions.

Ion Exchange Capacity

Ion Exchange Capacity (IEC) was measured immersing a specific amount of the membrane in a 1.0*M* solution of NaCl for 24 h. After removing the membrane, the solution was titrated using a 0.01*M* solution of NaOH until the pH was neutral. The IEC was calculated from the moles of ion substituted divided by the initial dry mass of the membrane.

Small Angle X-ray Scattering

The morphology of the membranes was carried out on a small angle X-ray scattering equipment from Anton Paar (SAXSpace). Two-dimensional scattering patterns were collected on a pinhole-collimated system using image plates and read by a Cyclone® Plus Perkin Elmer image plate reader. The SAXSQuant software® was used to reduce two-dimensional data to one-dimensional intensity versus scattering vector (Q) plots. The X-

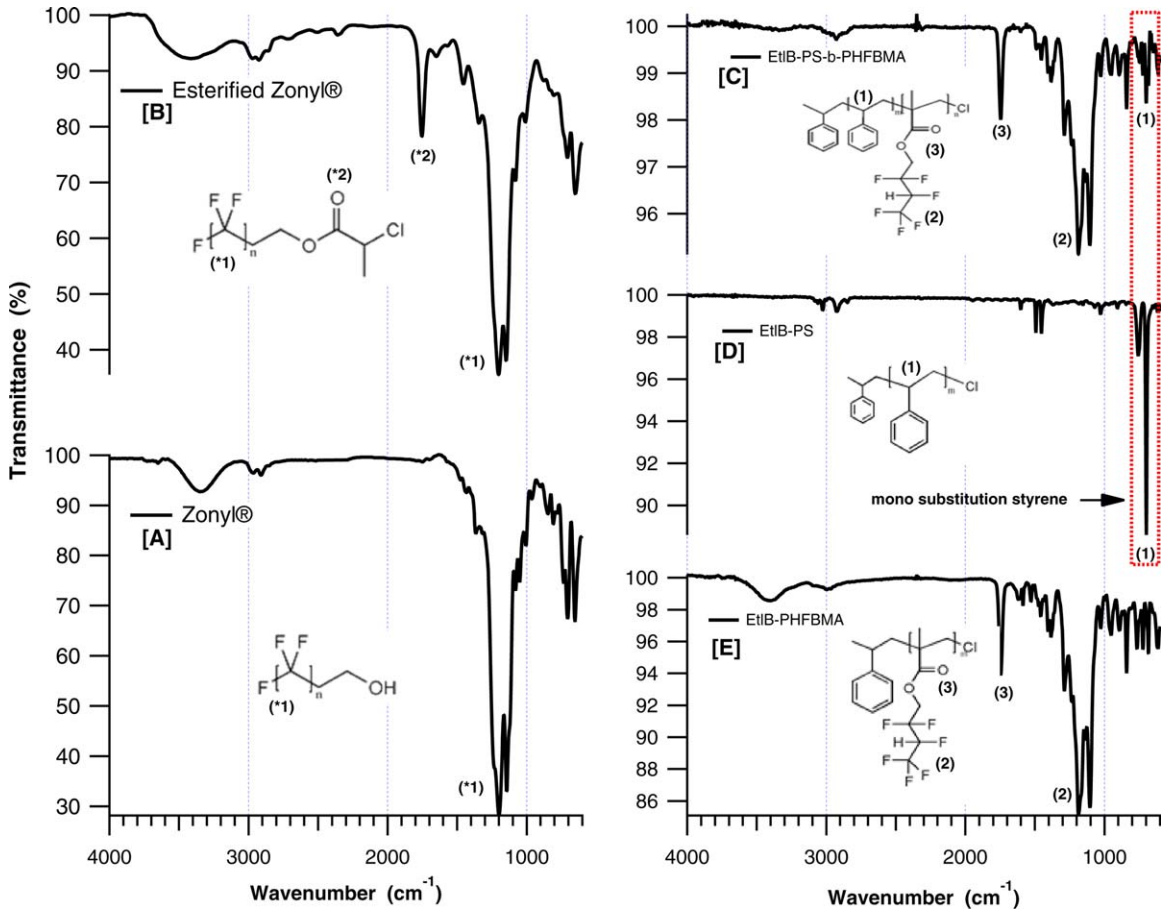

Figure 1. FTIR spectra for Zonyl® (A), esterified Zonyl® (B), EtIB-PS-b-PHFBMA (C), EtIB-PS (D), and EtIB-PHFBMA (E). [Color figure can be viewed in the online issue, which is available at wileyonlinelibrary.com.]

ray wavelength used was 1.54 Å. The calibration standard was silver behenate and the height of the beam stop was 0.3 mm.

RESULTS AND DISCUSSIONS

Polymer Characterization

FTIR Spectroscopy. Figure 1(A,B) presents the FTIR spectrum of Zonyl® and esterified Zonyl®; two distinctive bands were exhibited, the first band (*2) is attributed to the stretching vibration of the carbonyl group that appears around 1755 cm^{-1}. The second band (*1), corresponds to the polymer backbone (—CF2—), a strong band from 1100 to 1300 cm^{-1}, induced by the stretching vibration of the C—F groups.

Figure 1(D) shows the FT-IR spectra of EtIB-PS; two distinctive regions were observed in this figure. A monosubstitution band corresponding to the styrene group was presented at 700 cm^{-1} (1). The second bands correspond to the overtone absorptions induced by the aromatic ring; these bands appeared between 2000 and 1667 cm^{-1}. Figure 1(E) shows the FTIR spectra of EtIB-PHFBMA. This polymer presents a characteristic peak around 1750 cm^{-1} (3), that was ascribed to the stretching vibration of the carbonyl group attributed to the C═O bond attached to PHFBMA. Other important bands appeared from 1100 to 1300 cm^{-1} (2); these bands corresponded to the stretching vibration induced by the chemical presence of the fluoride groups incorporated by the polymerization reaction of PHFBMA. EtIB-PS-b-PHFBMA [Figure 1(C)] exhibited the stretching vibration of the carbonyl group attributed to the C═O bond attached to HFBMA around 1750 cm^{-1}. Other important bands corresponded to the stretching vibration induced by the chemical presence of the fluoride groups appeared from 1100 to 1300 cm^{-1}. The chemical presence of PS was confirmed by the monosubstitution band corresponding to this chemical group at 700 cm^{-1}. These results indicate the presence of PS and PHFBMA into the homopolymers and diblock fluoropolymer.

Figure 2(B) shows the FTIR spectra for Zonyl®-PS. This figure exhibited the monosubstitution band related to the styrene group and overtone absorptions induced by the aromatic ring appeared between 2000 and 1800 cm^{-1}. Zonyl®-PS-b-PHFBMA Figure 2(A) exhibited the same bands previously observed; additionally, the vibration of the carbonyl group attributed to the C═O bond appeared around 1750 cm^{-1} (3) and the fluoride group bands appeared from 1100 to 1300 cm^{-1} (2). Figure 2(D) shows the FT-IR spectra of Zonyl®-PHFBMA. The characteristic peak of the carbonyl group appeared around 1750 cm^{-1} (3) and, the bands corresponding to the fluoride groups

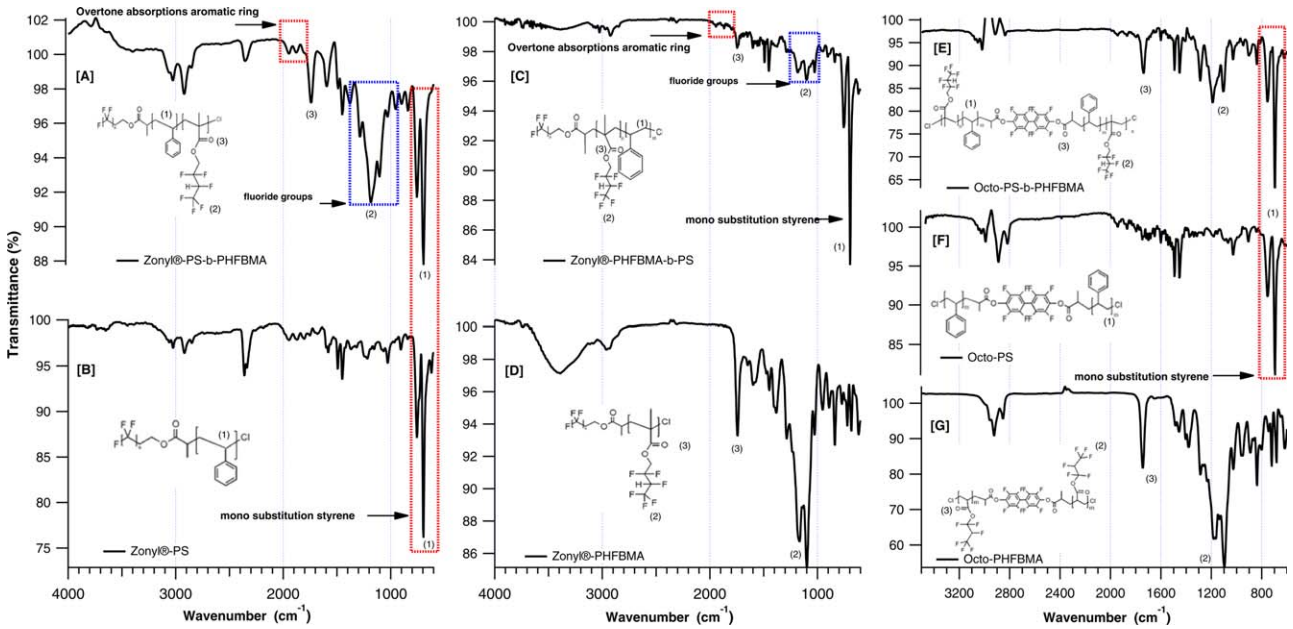

Figure 2. FTIR spectra Zonyl®-PS-b-PHFBMA (A), Zonyl®-PS (B), Zonyl®-PHFBMA-b-PS (C), Zonyl®-PHFBMA (D), octo-PS-b-PHFBMA (E), octo-PS (F), and octo-PHFBMA (G). [Color figure can be viewed in the online issue, which is available at wileyonlinelibrary.com.]

appeared from 1100 to 1300 cm^{-1} (2). Zonyl®-PHFBMA-b-PS Figure 2(C) presented similar chemical behavior as Zonyl®-PS-b-PHFBMA. This figure displays the overtone absorptions induced by the aromatic ring and the fluoride groups attached to PHFBMA. These bands evidence the chemical presence of PS and PHFBMA in the diblock copolymer. Differences between 2(A) and 2(C) could be due to the different block composition. Figure 2(E,F,G) present the FTIR spectra for octo-PS-b-PHFBMA, octo-PS, and octo-PHFBMA, respectively. These polymers also exhibited the characteristic bands of PS and PHFBMA in the range of wavenumbers previously mentioned.

Nuclear Magnetic Resonance. ^{1}H NMR was used to confirm the chemical composition of the synthesized homo and diblock fluoropolymers. Figure 3 exhibits the ^{1}H NMR spectra of EtlB-PS-b-PHFBMA Figure 3(B) and EtlB-PS Figure 3(A). EtlB-PS presented peaks at a large chemical shift around 7 ppm. These peaks (3) were assigned to the typical band of the protons attached to the aromatic ring in PS. The peaks at 1.85 and 1.5 ppm are assigned to the methylene (—CH2—) and methine (—CH—) resonances in PS. Three additional peaks appeared in EtlB-PS-b-PHFBMA with respect to PS at 4.95, 4.4, and 1 ppm, not previously present in PS. The resonance at 4.95 ppm is a

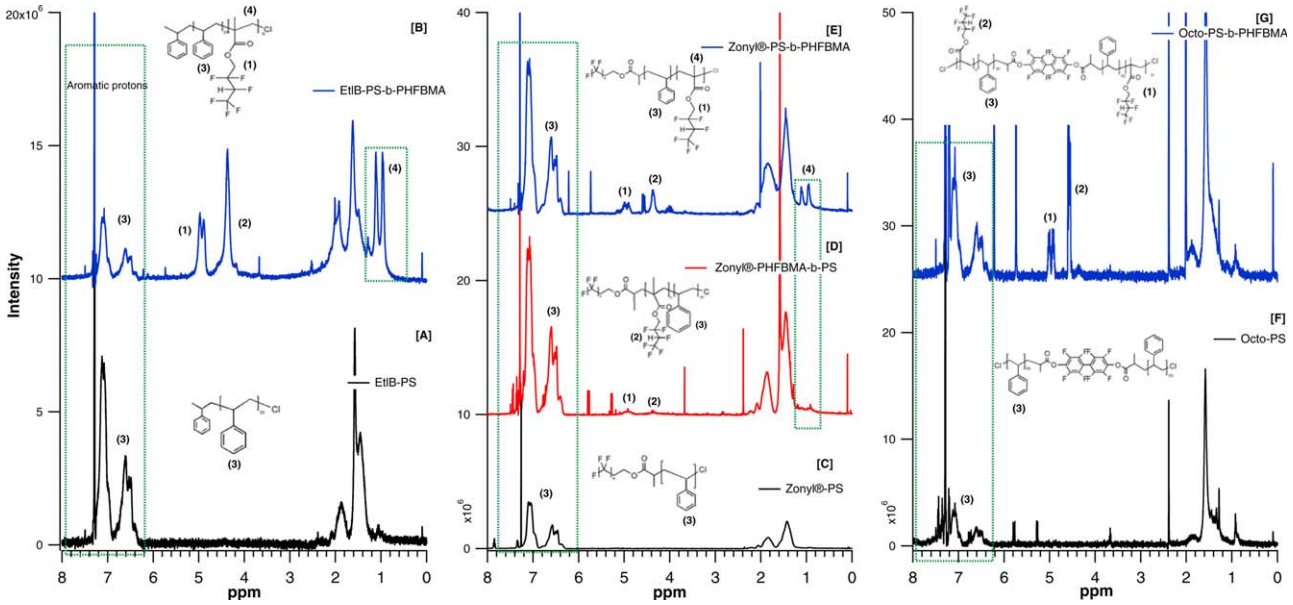

Figure 3. NMR spectra EtlB-PS-b-PHFBMA (A),EtlB-PS (B), Zonyl®-PS (C), Zonyl®-PHFBMA-b-PS (D), Zonyl®-PS-b-PHFBMA (E), octo-PS-b-PHFBMA (F), and octo-PS (G). [Color figure can be viewed in the online issue, which is available at wileyonlinelibrary.com.]

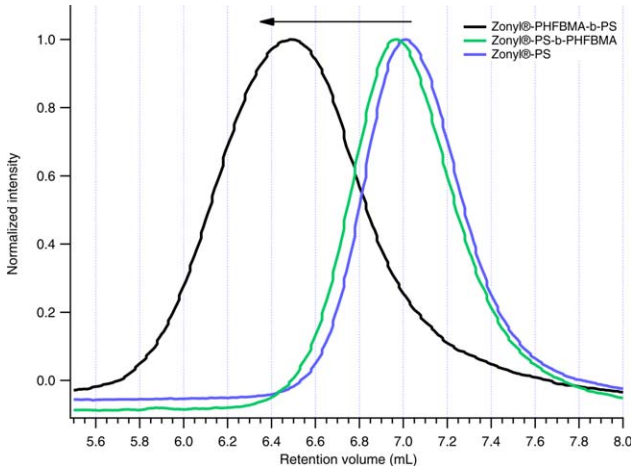

Figure 4. GPC traces of Zonyl®-PHFBMA-b-PS, Zonyl®-PS-b-PHFBMA, Zonyl®-PS. [Color figure can be viewed in the online issue, which is available at wileyonlinelibrary.com.]

characteristic chemical shift that corresponds to the hydrogens deshielded by the anisotropy of the adjacent C═O and fluorine groups, induced by the presence of PHFBMA in the diblock copolymer (1). The chemical shift at 4.4 ppm represents the proton attached to the same carbon as a fluorine group in PHFBMA (2). Methyl groups (—CH3—) peaks appeared at 1 ppm (4). The split of the methyl group resonance at 1 ppm is perhaps due to *m* and *r* dyads.

Zonyl®-PHFBMA-b-PS and, Zonyl®-PS-b-PHFBMA Figure 3(D,E) exhibited four similar characteristic peaks: a large chemical shift at 7 ppm related to the aromatic protons in PS, the hydrogens deshielded by the anisotropy of the adjacent C═O and fluorine groups at 4.95 ppm (1), the proton attached to the same carbon as a fluorine group in HFBMA (2), and the methyl groups (—CH3—) at 1 ppm.

Figure 3(F,G) present the NMR spectra for octo-PS and octo-PS-b-PHFBMA, respectively. The homopolymer and diblock copolymer synthesized presented the chemical shift, previously mentioned, and attributed to PS and PHFBMA. Both FT-IR and ^{1}H NMR spectra confirm that PS synthesized using three different initiators and their respective diblock copolymers were successfully prepared.

Gel Permeation Chromatography. The molecular weight of diblock copolymers were determined by GPC with THF as an eluent and PS as calibration standards. The GPC trace for Zonyl®-PS-b-PHFBMA, possess a higher retention volume that Zonyl®-PS (Figure 4); therefore, the diblock copolymer was obtained. The molecular weight for this block copolymer increased 11.3% with respect to Zonyl®-PS. The other homopolymers and diblock copolymers were successfully synthesized. The molecular weight, polydispersities (M_w/M_n) and the polymer composition results and are shown in Tables I and II.

Thermal Stability. The thermal stability for the homo and diblock copolymers was determined by thermogravimetric analysis (TGA) over a temperature range of 25–800°C under a N_2 atmosphere. In this report, the degradation temperature refers to the temperature when the higher degradation rate was achieved. The higher degradation rate is represented like a broad peak in the derivative curve from the TGA curve. For example, EtlB-PS shows one weight loss stage at 340–460°C and the degradation temperature is at 409°C Figure 5(B). The weight loss can be attributed to the PS backbone. Figure 5(C) presented the TGA curve for EtlB-PHFBMA. This polymer exhibited three weight loss stages at 120–195°C, 200–315°C, 320–420°C, respectively. Previous studies[36,37] have shown that methacrylic acid ester polymers suffered degradation at lower temperatures. These studies suggested that degradation mechanism at lower temperatures is related to the bond cleavage in the ester group (between the carbonyl group and oxygen)[38] and, the polymeric backbone degraded at higher temperatures. Figure 5(A) shows the TGA curve for EtlB-PS-b-PHFBMA. The

Table I. Molecular Weight Characterization for Homopolymer and Block Copolymers Prepared by ATRP (Using PS Standards)

Sample	Initiator	Mn × E−3	Mw × E−3	Mw/Mn
EtlB-PS	1-bromo ethyl benzene	3.68	5.19	1.41
EtlB-PS-b-PHFBMA	PS	24.9	48.2	1.94
Zonyl®-PS	Esterified Zonyl®	10.6	14.9	1.4
Zonyl®-PS-b-PHFBMA	Zonyl®-PS	11.8	16.9	1.44
Zonyl®-PHFBMA-b-PS	Zonyl®-PHFBMA	36.5	65.7	1.8
Octo-PS	Esterified octafluoro-4-4′-biphenol	24.6	42.3	1.7
Octo-PS-b-PHFBMA	Octo-PS	26.6	44.85	1.68

Table II. Polymer Composition (wt %)

Sample	Initiator (wt %)	PS (wt %)	PHFBMA (wt %)
EtIB-PS	3	97	Absent
EtIB-PS-b-PHFBMA	0.44	14.28	85.27
Zonyl®-PS	13.89	86.11	Absent
Zonyl®-PS-b-PHFBMA	8.98	55.52	35.50
Zonyl®-PHFBMA	2.99	Absent	97.01
Zonyl®-PHFBMA-b-PS	0.73	75.62	23.65
Octo-PS	10.81	89.19	Absent
Octo-PHFBMA	8.75	Absent	91.25
Octo-PS-b-PHFBMA	7.32	60.41	32.26

thermal stability of PS was adversely affected when PHFBMA was incorporated to the polymeric chain. Part of the fluorocarbon polymer group (ester group) suffered thermal degradation below 300°C and the remaining polymer chain degraded at 320–460°C. In this weight loss stage, the remaining of polymeric chain of PHFBMA and PS were overlapped.

PS initiated with esterified Zonyl® Figure 5(E) presented two weight loss stages of 14% and 85% at 145–280°C and 340–470°C, respectively. The incorporation of PHFBMA to Zonyl®-PS affected adversely the thermal stability of Zonyl®-PS-b-PHFBMA Figure 5(D). This polymer shows three different degradation temperatures at 212, 279, and 405°C with 15, 9, and 75% of weight loss, respectively. Furthermore, Zonyl®-PS-b-PHFBMA started its degradation at a lower temperature than EtIB-PS-b-PHFBMA. Figure 5(F) shows the TGA for Zonyl®-PHFBMA. This polymer exhibited only one weight loss stage at lower temperatures, while EtIB-PHFBMA exhibited two different weight loss stages. The remaining polymeric back-bone degrades at similar degradation temperature for both polymers. Additionally, the incorporation of PS to Zonyl®-PHFBMA improved the thermal stability at higher temperatures; however, the weight loss stages at lower temperatures (corresponding to PHFBMA), was still present.

Octo-PS Figure 5(H) presented a weight loss stage of 11% at 140–260°C and another at 340–480°C. Octo-PHFBMA Figure 5(I) exhibited changes in the TGA curve with respect to EtIB-PHFBMA and Zonyl®-PHFBMA. A large weight loss of 58% appeared at 180–300°C and remaining of the polymeric chain degraded at 320–420°C. Figure 5(G) presents the TGA curve for octo-PS-b-PHFBMA; this polymer presented a large weight loss of 37% at 125–300°C and the remaining of polymeric chain degraded at 340–480°C. These results suggest that the degradation behavior remarkably depends on the initiator; therefore, the incorporation of esterified Zonyl® or esterified octafluoro 4-4′-biphenol to PS or PHFBMA thermally destabilizes the polymeric chain, presenting an additional weight loss at lower temperature with respect to the homopolymer initiated with 1-bromo ethyl benzene. Table III summarizes the degradation temperatures for all the synthesized polymers.

Effect of the Chemical Nature of the Initiator on the Electronic Transitions and Thermal Stability. To investigate the role of the initiators on the thermal stability of the polymers, EtIB-PS-b-PHFBMA and Zonyl®-PS were exchanged with a solution 0.1*M* of NaOH for 48 h and then their thermal behavior were obtained. Studies suggest that the interactions of the counter-ion with a specific group, like ethers[18] or the sulfonic group[15,16,39] improve the polymer stability. A unique feature was observed for EtIB-PS-b-PHFBMA exchanged with Na^{+1} Figure 6(A). Although the polymer backbone degraded at the same temperature, the first degradation region, (corresponding to the ester group), was absent; moreover, the second degradation

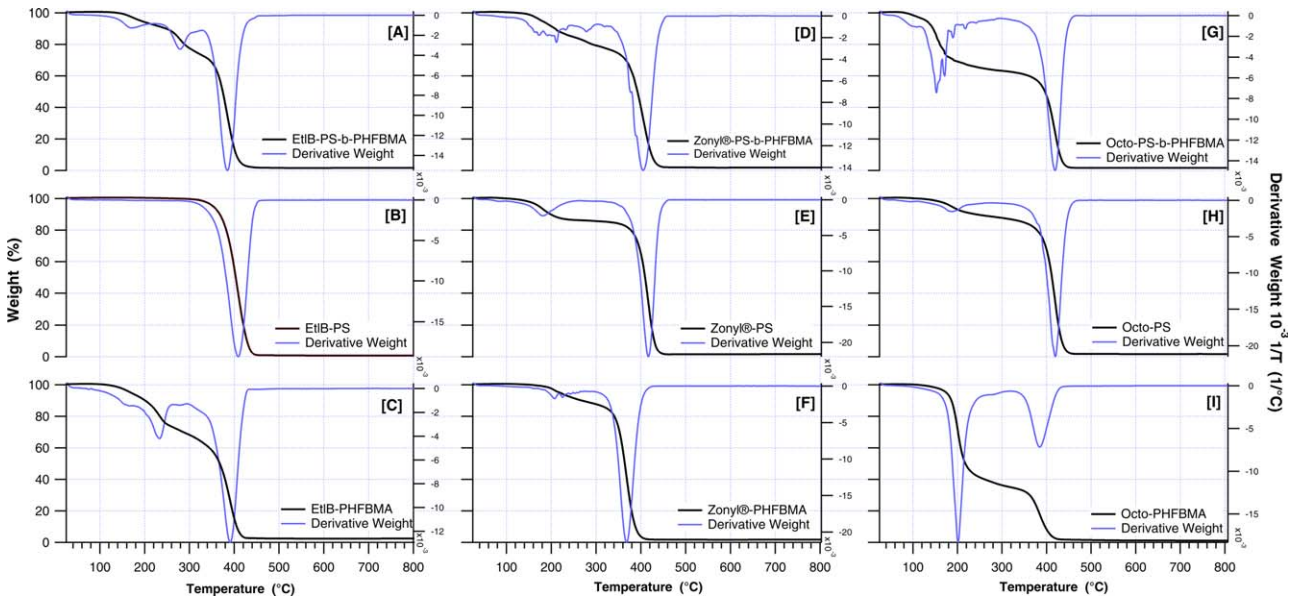

Figure 5. TGA for EtIB-PS-b-PHFBMA (A), EtIB-PS (B), EtIB-PHFBMA (C), Zonyl®-PS-b-PHFBMA (D), Zonyl®-PS (E), Zonyl®-PHFBMA (F), octo-PS-b-PHFBMA (G), octo-PS (H), and octo-PHFBMA (I). [Color figure can be viewed in the online issue, which is available at wileyonlinelibrary.com.]

Table III. Polymer and Initiators Degradation Temperatures

Polymer	1st degradation (°C)	Weight (%)	2nd degradation (°C)	Weight (%)	3rd degradation (°C)	Weight (%)	Residue (%)
Zonyl®-PS-b-PHFBMA	212	15	279	9	402	75	1
Zonyl®-PS	182	14	Absent	Absent	417	85	1
Zonyl®-PS-Na	260	10	Absent	Absent	412	89	1
Zonyl®-PHFBMA-b-PS	124	3	199	7	419	89	1
Zonyl®-PHFBMA	208	12	Absent	Absent	368	87	1
Esterified Zonyl®	174	89	297	4	Absent	Absent	7
Zonyl®	170	99.85	Absent	Absent	Absent	Absent	0.15
Octo-PS-b-PHFBMA	153	37	Absent	Absent	420	62	1
Octo-PS	188	11	Absent	Absent	420	88	1
Octo-PHFBMA	202	58	Absent	Absent	385	41	1
Esterified octafluoro-4-4′-biphenol	265	89	Absent	Absent	450	10	1
Octafluoro-4-4′-biphenol	130	8	220	91	Absent	Absent	1
EtIB-PS-b-PHFBMA	172	8	280	18	385	72	2
EtIB-PS-b-PHFBMA-Na	Absent	Absent	280	13	382	86	1
EtIB-PS	Absent	Absent	Absent	Absent	408.86	99.84	0.16
EtIB-PHFBMA	167	9	233	23	391	65	3

(related also to ester group) suffered 13% of weight loss, instead of 18% without the counter ion-substitution. This suggests that sodium interacts directly with the ester group improving the thermal stability of this polymer. A similar procedure was used with Zonyl®-PS; the thermal stability of this polymer significantly improved (78°C) after the counter-ion substitution with sodium Figure 6(C). These results suggest that the counter-ion inhibited the bond cleavage in the ester group contained in the

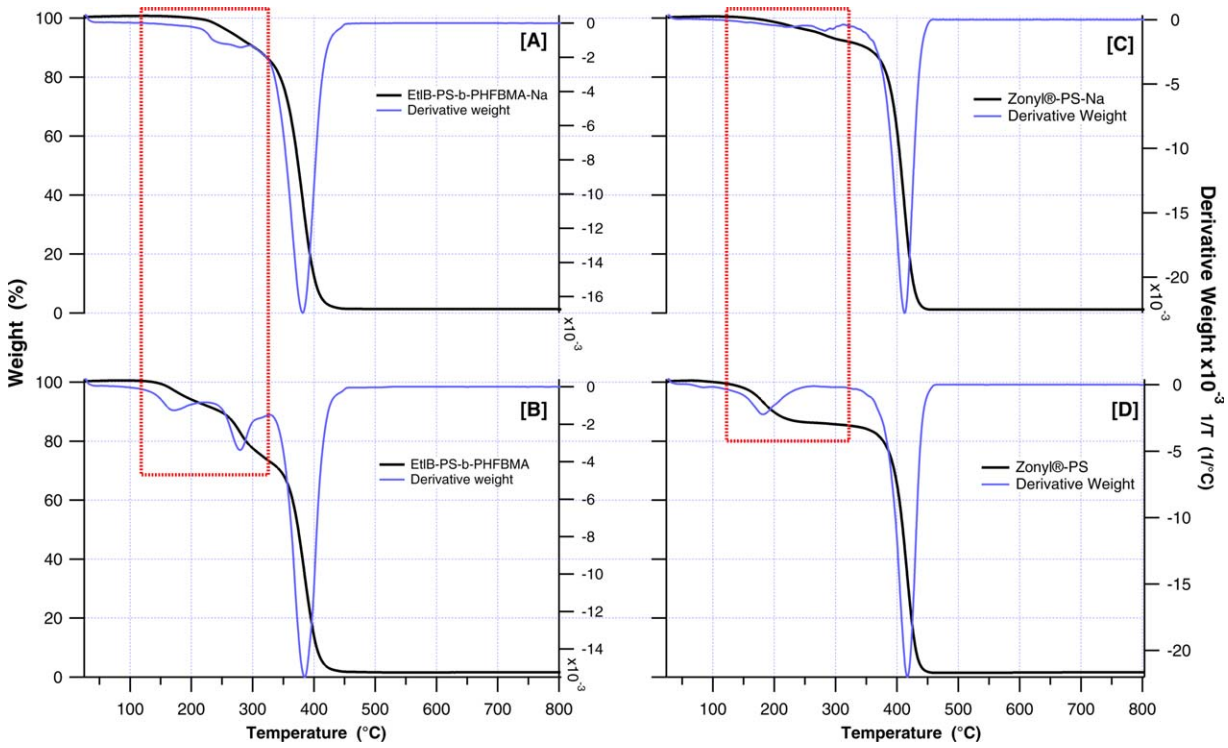

Figure 6. TGA for EtIB-PS-b-PHFBMA-Na (A), EtIB-PS-b-PHFBMA (B), Zonyl®-PS-Na (C), and Zonyl®-PS (D). [Color figure can be viewed in the online issue, which is available at wileyonlinelibrary.com.]

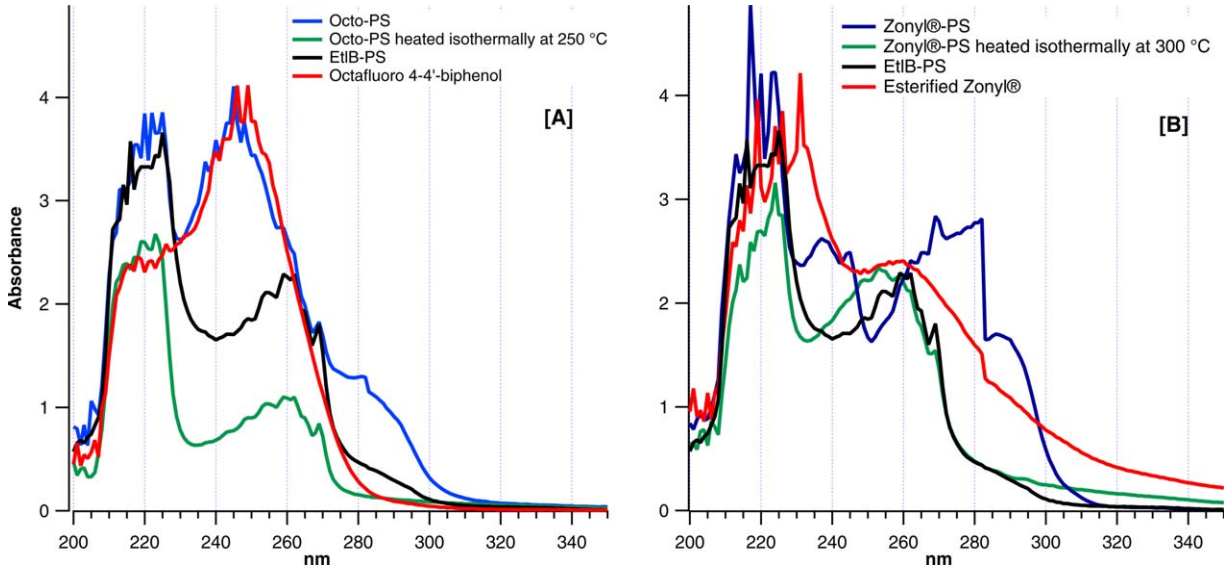

Figure 7. UV comparison between octo-PS, octo-PS heated isothermally at 250°C during 2.5 h, EtIB-PS, octafluoro 4-4′-biphenol (A) and Zonyl®-PS, Zonyl®-PS heated isothermally at 300°C during 2.5 h, EtIB-PS and esterified Zonyl® (B). All the UV spectra were measured at room temperature. [Color figure can be viewed in the online issue, which is available at wileyonlinelibrary.com.]

esterified Zonyl®. Other experiments are presented ahead to understand the impact of the initiator on the thermal stability of these polymers.

The electronic transitions and thermal stability of the polymers were investigated with UV spectroscopy at room temperature. In this experiment, the polymer was heated isothermally at a specific temperature (e.g., 250 or 300°C) during two and a half hours. The resulting polymers were dissolved in THF and then the UV spectrum were recorded and analyzed. The UV spectrum of octafluoro-4-4′-biphenol, EtIB-PS and octo-PS isothermally heated to 250°C, are presented in Figure 7(A). This figure also shows the UV spectrum for octo-PS for comparison purposes. As shown in this figure, octafluoro-4-4′-biphenol exhibited a lambda maxima at 247 nm, which corresponds to the secondary band of the aromatic rings attached to the diphenol group. The 220-nm band is less intense, and it corresponds to a forbidden transition of the aromatic ring.[40] PS initiated with 1-bromo ethyl benzene presented two typical transitions related to the aromatic ring present in styrene. The band at 260 nm corresponds to the transition related to the secondary bands of the aromatic ring; another band at 225 nm is associated with the primary bands of this chemical group attached into this polymer.

The incorporation of octafluoro-4-4′-biphenol into the polymeric chain of PS produced a unique and different UV spectrum than PS initiated with 1-bromo ethyl benzene. Octo-PS presented a lambda maxima at 245 nm, this band corresponds to the transition related to the secondary band of the aromatic ring attached to the diphenol group presented in the initiator. The observed spectrum for this polymer has an additional absorption band around 280–290 nm, this band is attributed to the $n - \pi^*$ transition of the carbonyl group[40–42] attached to the octafluoro-4-4′-biphenol after the esterification reaction. The

Table IV. UV Parameters

Polymer	λ1 (nm)	λ2 (nm)	λ3 (nm)	λ4 (nm)	λ5 (nm)
EtIB-PS	220	Absent	Absent	260	Absent
EtIB-PS-b-PHFBMA	220	237.5	245	260	282
Zonyl®-PS	220	237.5	245	260	282
Zonyl®-PS heated isothermally at 300°C	220	Absent	Absent	255	Absent
Zonyl®-PS-b-PHFBMA	220	237.5	245	260	282
Esterified Zonyl®	220	232	Absent	258	282
Zonyl®	220	232	Absent	258	Absent
Octo-PS-b-PHFBMA	220	237.5	245	Absent	282
Octo-PS	220	Absent	245	Absent	282
Octo-PS heated isothermally at 250°C	220	Absent	Absent	260	Absent
Esterified octafluoro-4-4′-biphenol	220	Absent	247	Absent	282
Octafluoro-4-4′-biphenol	220	Absent	247	Absent	Absent

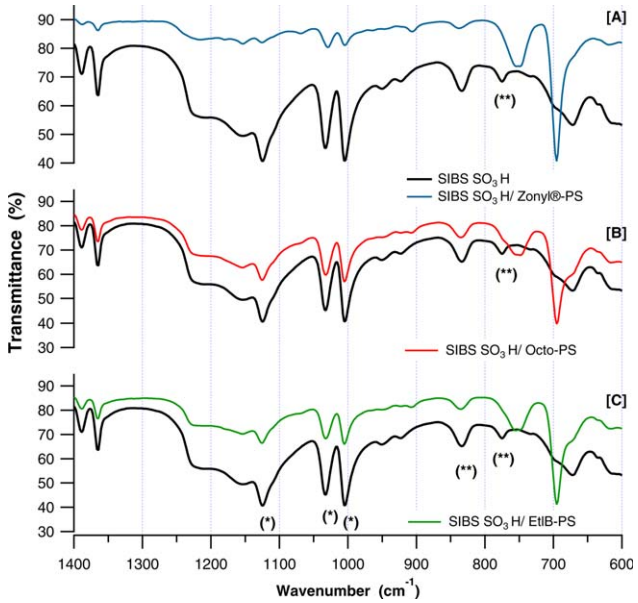

Figure 8. FTIR spectra for SIBS SO_3H/ Zonyl®-PS (A), SIBS SO_3H / octo-PS (B), and SIBS SO_3H / EtIB-PS (C). [Color figure can be viewed in the online issue, which is available at wileyonlinelibrary.com.]

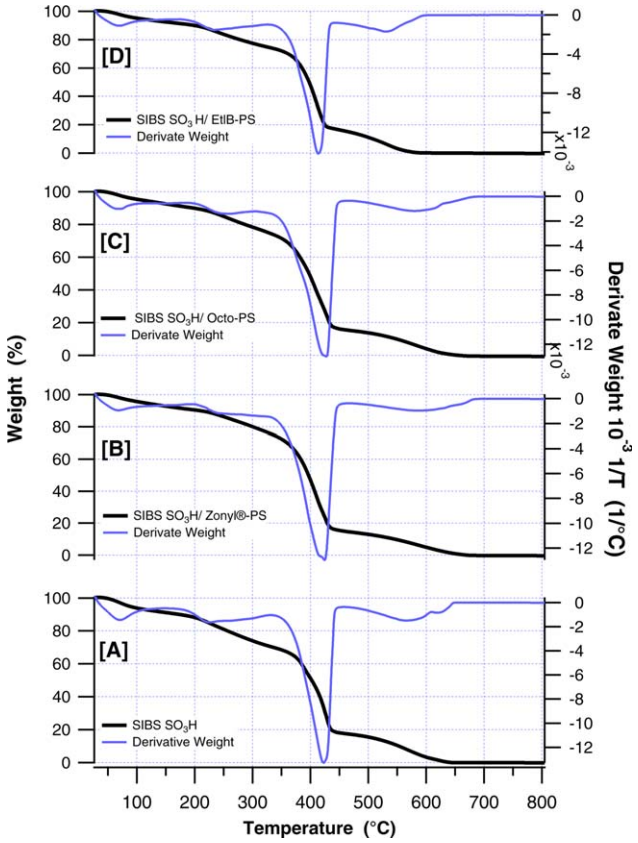

Figure 9. TGA for SIBS SO_3H (A), SIBS SO_3H/ Zonyl®-PS (B), SIBS SO_3H / octo-PS (C), and SIBS SO_3H / EtIB-PS (D). [Color figure can be viewed in the online issue, which is available at wileyonlinelibrary.com.]

bands corresponding to the PS group in this polymer are overlapped at 260 nm with the band related to the diphenol group present in the initiator.

Octo-PS was heated isothermally at 250°C, after this process, the UV spectrum was recorded. The observed spectrum for this polymer shows that the heat treatment removed the bands attributed to the $n - \pi^*$ transition of the carbonyl group attached in the initiator. In addition, the band at 245 nm assigned to diphenol group in the initiator disappeared. These results suggests that the first weight loss of octo-PS presented in the TGA curve correspond to the esterified octafluoro-4-4′-biphenol.

Similarly PS initiated with esterified Zonyl® was analyzed. Figure 7(B) presents the UV spectrum for esterified Zonyl®, EtIB-PS and Zonyl®-PS heated isothermally to 300°C. As shown in this figure, Zonyl®-PS exhibited an absorption band around 280–290 nm; this band is also attributed to the $n - \pi^*$ transition of the carbonyl group attached to this initiator. The PS group exhibited a band at 260 nm related to the aromatic ring. A similar procedure was used to understand the thermal effect of the esterified Zonyl® on PS: it was heated isothermally at 300°C during two and a half hours; after this process the UV spectrum was recorded and analyzed. The UV spectrum exhibited that the heat treatment also removed the bands attributed to the n – π^* transition of the carbonyl group attached to the initiator; additionally, the bands at 235 and 245 nm disappeared. The spectrum obtained after the heat treatment shows a similar trend to that observed for PS. These results suggest that the first weight loss of Zonyl®-PS presented in the TGA curve corresponds to the esterified Zonyl®.

Table IV summarized the UV transitions for all the polymer synthesized with the different initiators and the diblock copolymers. As shown in this table, octo-PS and octo-PHFBMA for example, exhibited a strong absorption at 245 nm. This absorption was related to the esterified octafluoro 4-4′-biphenol in the polymer. The bands corresponding

Table V. FTIR Stretching Vibration Bands for Polymeric Blends Membranes

Membrane	FTIR bands (cm−1)		
SIBS SO_3H	1124	1034	1005
SIBS SO_3H/ EtIB-PS	1126	1032	1005
SIBS SO_3H/ Zonyl®-PS	1126	1027	1005
SIBS SO_3H/ Octo-PS	1126	1032	1005

Table VI. Degradation Temperatures for the Polymeric Blend Membranes

Membrane	2nd Degradation (°C)	3th Degradation (°C)	4th Degradation (°C)
SIBS SO_3H	220	405	565
SIBS SO_3H/ EtIB-PS	233	414	530
SIBS SO_3H/ Zonyl®-PS	244	425	586
SIBS SO_3H/ Octo-PS	258	427	580

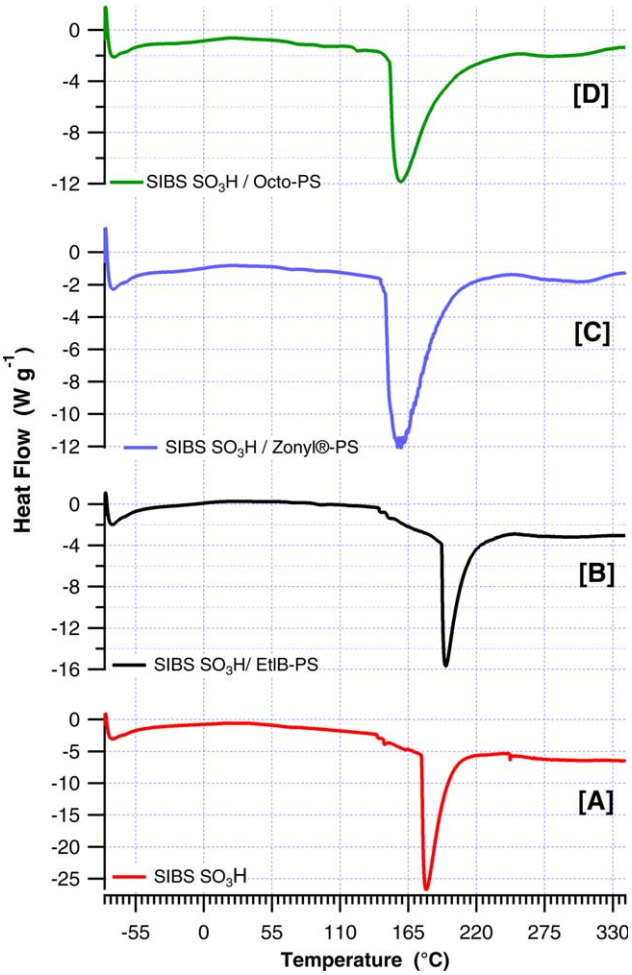

Figure 10. DSC for SIBS SO_3H (A), SIBS SO_3H / EtIB-PS (B), SIBS SO_3H/ Zonyl®-PS (C), and SIBS SO_3H / octo-PS (D). [Color figure can be viewed in the online issue, which is available at wileyonlinelibrary.com.]

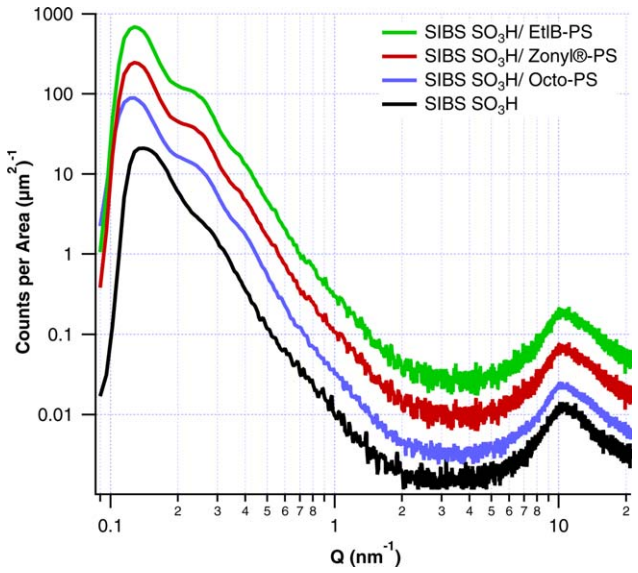

Figure 11. A log–log SAXS profile for polymeric membranes. [Color figure can be viewed in the online issue, which is available at wileyonlinelibrary.com.]

to PS and PHFBMA were overlapped by this absorption. These results suggest that the initiator produced unique UV spectrum for these polymers depending on the chemical properties of the initiator.

Polymer Blend Characterization

Fluoropolymer Interaction with the SIBS SO_3H. Figure 8(A) shows the FT-IR spectrum of SIBS SO_3H and SIBS SO_3H / Zonyl®-PS membranes. SIBS SO_3H membrane exhibited three distinctive bands at 1124, 1034, 1007 (*) cm^{-1} associated to the sulfonic group.[15] The band at 1034 cm^{-1} was caused by an symmetric stretching vibration of the sulfonated group attributed to the S=O bond. Other important bands correspond to the para-substitution of the sulfonic group at 830 cm^{-1}(**) and the monosubstitution of the aromatic ring in PS at 770 cm^{-1}(**).[15] This figure also shows the FTIR for SIBS SO_3H / Zonyl®-PS membrane; the addition of this polymer to SIBS SO_3H membrane shifts the symmetric stretching vibration of the S=O group toward lower wavenumbers; however, the band corresponding to the monosubstitution disappeared. These results suggest that the Zonyl®-PS is interacting with the sulfonic group and the aromatic ring; therefore, a change of energy is required to produce the bands at those specific wavenumbers. Figure 8(B) shows the FTIR spectrum of SIBS SO_3H and SIBS SO_3H / Octo-PS membranes. The incorporation of this polymer to SIBS SO_3H membrane also shifted the symmetric stretching vibration of the S=O group and the monosubstitution band, suggesting an interaction between the sulfonic group and the aromatic ring with Octo-PS. The incorporation of EtIB-PS to SIBS SO_3H membranes presented the same behavior previously mentioned; the polymer changed the symmetric vibration of the sulfonic group toward lower wavenumber Figure 8(C). Other experiments are presented ahead to understand the impact of the incorporation of these polymers in SIBS SO_3H membranes. Table V summarizes the wavenumber changes for the symmetric stretching vibration of the sulfonic group.

Table VII. Endothermic Transition Temperatures for Polymeric Blend Membranes

	First transition		Second transition	
Membrane	T (°C)	ΔH (J g^{-1})	T (°C)	ΔH (J g^{-1})
SIBS SO_3H	146	1.30	180	208.5
SIBS SO_3H/ EtIB-PS	Absent	Absent	195	149.1
SIBS SO_3H/ Zonyl®-PS	Absent	Absent	159	221.6
SIBS SO_3H/ Octo-PS	123	0.40	159	208.9

Thermal Stability. Figure 9(A) shows the TGA curve for SIBS SO_3H. The TGA curve for this membrane exhibited four weight loss stages, the first one at 50–100°C corresponds to water absorbed inside the membrane. The second degradation region at 200–350°C corresponds to the degradation of the sulfonic group. The third degradation at 350–450°C represents the polymer backbone degradation, as well as the last degradation at

Table VIII. Scattering Vector, Bragg Distance, and Radius of Gyration for the Polymeric Blend Membranes

Membrane	Q_{1Bragg} (nm^{-1})	d_{1Bragg} (nm)	Q_{2Bragg} (nm^{-1})	d_{2Bragg} (nm)	Q_{3Bragg} (nm^{-1})	d_{3Bragg} (nm)	Radius of gyration (nm)
SIBS SO_3H	0.141	44.56	Absent	Absent	Absent	Absent	14.66
SIBS SO_3H / EtlB-PS	0.128	49.08	0.230	2.73	0.256	2.45	17.45
SIBS SO_3H / Zonyl®-PS	0.128	49.08	0.230	2.73	0.256	2.45	17.45
SIBS SO_3H / Octo-PS	0.128	49.08	Absent	Absent	0.243	2.58	16.72

450–650°C.[16,39] Figure 9(B) shows the TGA curve for SIBS SO_3H / Zonyl®-PS membrane. The incorporation of this polymer to SIBS SO_3 improved 24°C the sulfonic group degradation, 11°C the polymer backbone degradation, and 56°C the last degradation. Ionic interactions with the sulfonic group in SIBS SO_3H membranes produced an improvement in the second and last degradation temperature in this membrane.[16] SIBS SO_3H / Octo-PS Figure 9(C) and SIBS SO_3H / EtlB-PS Figure 9(D) improved 38°C and 13°C the sulfonic group degradation and 22°C and 9°C the polymer backbone; however, SIBS SO_3H / EtlB-PS reduced the last degradation 35°C. Table VI summarized the degradation temperatures for the polymeric blend membranes.

Effect of the Chemical Nature of the Initiator on the Morphology. To understand the effect of the initiator on the morphology, DSC curves and SAXS profiles were obtained. Figure 10(A) shows the DSC curve for SIBS SO_3H. Sulfonated SIBS presents the two endothermic transitions induced by the sulfonation process; the first at 140°C and the second at 177°C. The incorporation of the fluoroblock copolymer to the SIBS SO_3H membrane produced unique DSC curves for each of the polymer studied. SIBS SO_3H / EtlB-PS Figure 10(B) presented a difference in both the energy and temperature required to produce the endothermic transitions. The first endothermic transitions disappeared, however the second endothermic transition shifted toward higher temperature and the energy required for this transition was reduced. These changes in temperature are related to the energy needed to overcome the crystalline bonding forces and changes in the molecular conformation of the chains in the polymer.[43] DSC results for sulfonated membranes show that changes in the energy and temperature required to produce the endothermic transition for the ionic group (first endothermic transition) and crystalline regions (second endothermic transition) are associated to a new configuration for the ionic domain and the polymeric backbone.[18] SIBS SO_3H / Zonyl®-PS Figure 10(C) also presented changes in the temperature and energy required to produce the endothermic transitions. This membrane required more energy to produce the endothermic transition for the crystalline region than SIBS SO_3H and SIBS SO_3H / EtlB-PS; however the transition for the ionic domain disappeared. SIBS SO_3H / Octo-PS exhibits the ionic and the crystalline transitions; however both transitions were shifted to lower temperatures than SIBS SO_3H Figure 10(D). Table VII summarizes the endothermic transition temperatures and their corresponding energies for the membranes studied. The second endothermic transition is often considered a melting temperature (T_m).

Sulfonated SIBS has a highly ordered sequence of ionic and nonionic blocks which self-assemble into a three-phase nanostructured morphology in the solid state. Studies suggest that sulfonated SIBS with ion content between 0.5 and 1 mequiv g^{-1} exhibited in the SAXS profiles, reflections at the vector

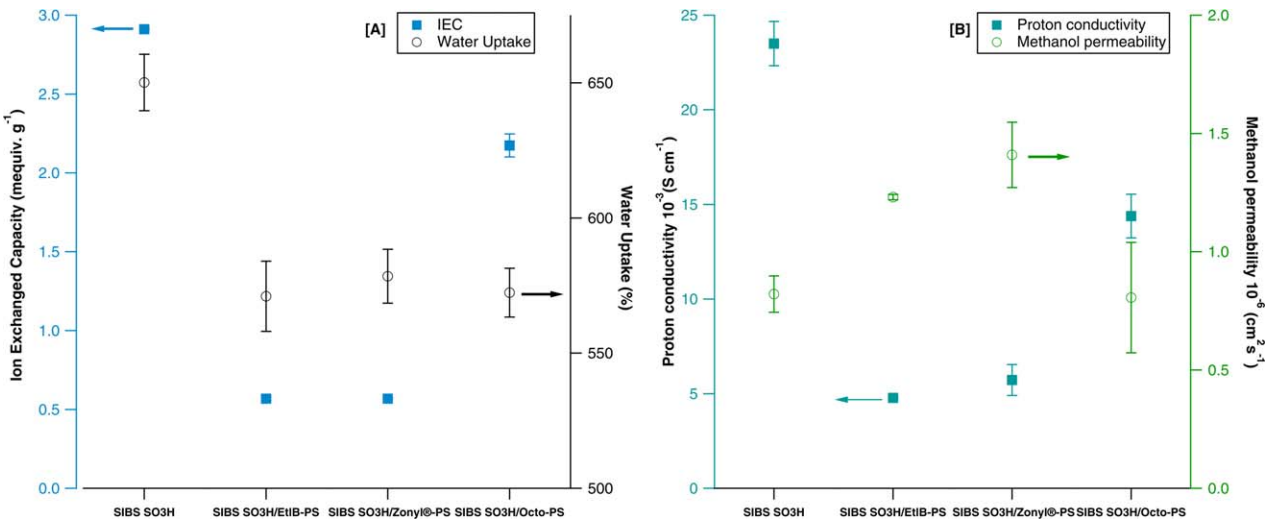

Figure 12. Ion Exchanged Capacity and water uptake (A) and proton conductivity and methanol permeability (B) for polymeric membranes. [Color figure can be viewed in the online issue, which is available at wileyonlinelibrary.com.]

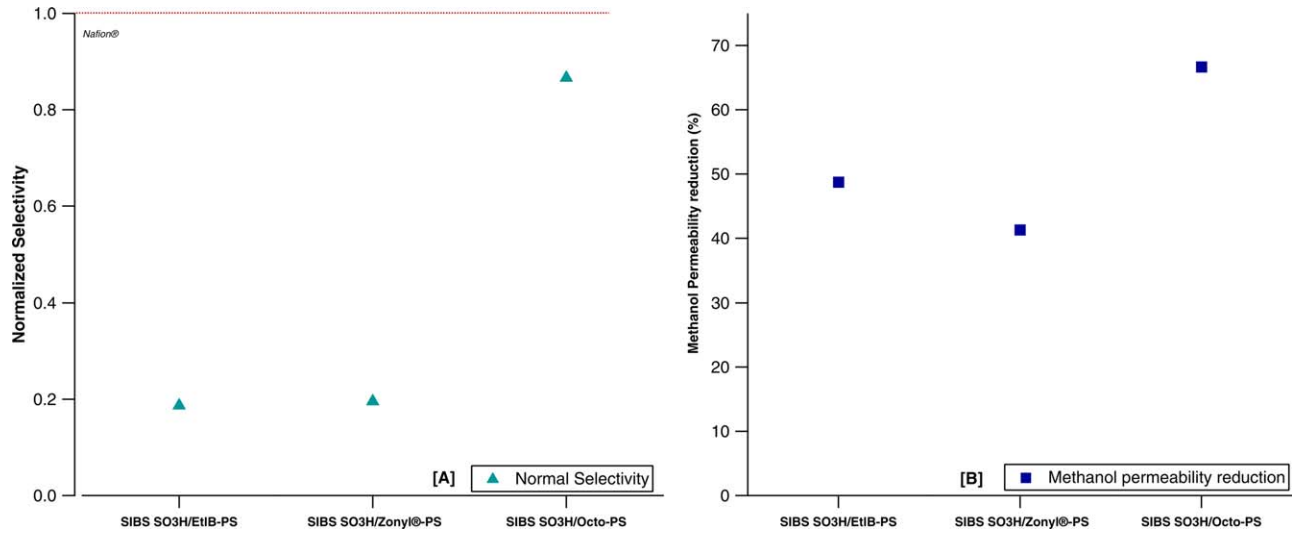

Figure 13. Normalized Selectivity (Proton Conductivity / Methanol Permeability) for polymeric blends with different initiators (Normalized with selectivity of Nafion®) (A) and methanol permeability reduction (B). [Color figure can be viewed in the online issue, which is available at wileyonlinelibrary.com.]

positions: q_1, $2q_1$, $3q_1$, $4q_1$, $5q_1$, and $6q_1$, that correspond to a laminar morphology; however, as the ion content increased above 1 mequiv g^{-1}, the membrane exhibited a nonperiodic morphology at higher ion content.[44] Other sulfonated membranes with intermediate sulfonation levels of 58 and 81% also showed a similar behavior, suggesting that differences in the solubility parameter between the sulfonic group, the PS and the polymer backbone leads to phase segregation which impacts the morphology.[45] Figure 11 shows the SAXS spectra SIBS SO_3H / polymers with a sulfonation level of 81%. SIBS SO_3H exhibited a first-order reflection at $Q = 0.141$ nm^{-1}. The incorporation of the fluoroblock copolymer to the SIBS SO_3H shifted the first order reflection toward lower scattering vector at $Q = 0.128$ nm^{-1}. The incorporation of EtlB-PS induced a morphological change in SIBS SO_3H membranes; two additional peaks appeared at $Q = 0.23$ and 0.256 nm^{-1} Combining Bragg's law with the scattering vector (Q) obtained from the SAXS plot, the interstitial distance was determined from the maximum in the first-order reflection and the additional peaks. The Bragg's distance for the first order reflection, increases with the incorporation of the fluorinated polymers from 44.56 to 49.09 nm (Table VIII).

Another important parameter that was obtained from the SAXS data was the radius of gyration (R_g). For polymers, this parameter represents the distance from the center of mass and can be used to evaluate changes with the different initiators studied. This parameter was obtained using the Guinier equation, which provides the relation between Rg, the intensity in a SAXS profile and the scattering vector (Q). R_g was estimated using the slope of the linear relationship between $Ln(I(Q))$ and Q^2.[46] The incorporation of PS with different initiators into the SIBS SO_3H membrane produced unique R_g's (Table VIII). The use of ethyl benzene and esterified Zonyl® as initiators increased Rg by 19% from SIBS SO_3H; however, the Octo-initiated polymer increased R_g by only 14%. These results are related to the changes induced by the incorporation of the polymer on the molecular conformation of the polymeric chains and sulfonic group in the membrane showed in the FTIR and TGA experiments.

Effect of the Chemical Nature of the Initiator on the Transport Properties. ***Ion exchange capacity and water uptake.*** Fig-. Figure 12(A) presents IEC and water uptake for the polymer membranes studied. SIBS SO_3H had the highest IEC and water swelling. On the incorporation of PS with different initiators, the amount of water remained constant, although lower than SIBS SO_3H. The IEC for the octo-initiated PS was significantly higher than with the other initiators. Das *et al.*,[47] explained a reduction in the IEC of sulfonated fluorinated polymers with the formation of cross-linked chemical groups. Moukheiber *et al.*,[48] studying perfluoro sulfonic membranes found-out that IEC changed with the distance between the ionic domains and the polymer length. Elabd *et al.*,[44] suggested that morphological changes can also lead to changes in IEC. Our results for SIBS SO_3H / EtlB-PS and SIBS SO_3H / Zonyl®-b-PS show a significant reduction in IEC, perhaps due to the additional phase segregation on the incorporation of the PS that perhaps led to the cross-linking of the sulfonic domains. SIBS SO_3H / Octo-PS showed a much lower reduction in IEC from SIBS SO_3H, and significantly higher than the other initiated PS perhaps due to the chemical nature of the esterified octo initiator that allowed polymerization from the center in both directions. In addition, as our UV results point-out a significant electronic transitions for the octo-initiated polymer, this can lead to an improved electron mobility as suggested by Dutta *et al.*[49]

Proton conductivity and methanol permeability. Proton conductivity and methanol permeability for SIBS SO_3H, SIBS SO_3H/ EtlB-PS, SIBS SO_3H / Zonyl®-PS and SIBS SO_3H / Octo-PS membranes are presented in Figure 12(B). SIBS SO_3H / Octo-PS presents the highest value of proton conductivity (three times higher) for the three different initiators evaluated, even though its water uptake was very similar to the other initiators. SIBS SO_3H / Octo-PS however, had the highest IEC among the

initiators studied, suggesting that the initiator octo influenced new ionic conformations that improved the transport of protons through the membrane. These results agree with other proton conductivity results, where proton conductivity is related with IEC.[50–52] The transport of protons used the hydrated sulfonic groups in the polymeric membrane; the predominant mechanism consists in a series of Eigen-Zundel-Eigen or Zundel-Zundel transformations that depend on the sulfonic group,[53] the type of water,[54] and the morphology.[45] The incorporation of the polymer produced a reordering of polymeric chains and the ionic domain for SIBS SO_3H membranes. The polymer interacts with the ionic domains that inhibit the complex formation between the proton, water and the sulfonic group described above.

The methanol permeability of the polymeric blend membranes are also presented in Figure 12(B). The methanol permeability for SIBS SO_3H/ EtlB-PS, SIBS SO_3H/Zonyl®-PS and SIBS SO_3H/Octo-PS increased or remain the same in comparison with SIBS SO_3H. One possible explanation for this behavior could be related to the increase in free volume, concluded from the SAXS results (Rg). The methanol permeability in an ionic polymeric membrane is influenced by the capacity of the compound to move through the free volume available,[55] the morphology[45,50] and the sulfonic group configuration.[15–18]

These results agree with the previously presented DSC, FTIR, TGA, IEC, and SAXS results, where the variation of the proton conductivity and methanol permeability for each membrane is related to the interaction between the fluoroblock copolymer with SIBS SO_3H, the changes in the sulfonic group conformation, and changes in morphology (related to its free volume) induced by the different initiators used.

To evaluate the effect of each initiator on the transport properties of protons and methanol, and to compare the changes with respect to the state-of-the-art Nafion®, a normalized selectivity was calculated. Figure 13(A) presents the normalized selectivity (Proton Conductivity / Methanol Permeability) for the blend membranes (normalized with the values for Nafion®). The results show that the highest selectivity, corresponds to SIBS SO_3H/Octo-PS membrane; this selectivity although slightly lower than Nafion® (13.4% lower), is comparable. In addition, Figure 13(B) shows a significant reduction in the methanol permeability from Nafion® and the significant variations with the choice of initiator for DMFC applications.

CONCLUSIONS

Four novel diblock fluoropolymers and their homopolymers were successfully synthesized using two fluorinated initiators (esterified Zonyl® and esterified octafluoro 4-4′-biphenol) and 1-bromo ethyl benzene by ATRP. The selection of the esterified initiators has a significant impact on the thermal stability of PS, PHFBMA and the diblock copolymers. The thermal stability of PS was reduced on polymerization with esterified initiators. Additionally, an additional degradation was observed with the new esterified initiator around 150°C. This degradation temperature was absent when 1-bromo ethyl benzene was used. Furthermore, different UV spectrum was obtained for PS and PHFBMA depending on the initiator used. The use of different esterified initiators with sulfonated SIBS influenced the ionic domains uniquely, which influenced the IEC, the water swelling, the morphology and the transport of protons and methanol through the membrane. Therefore, the proton conductivity and methanol permeability of these membranes is limited by the nature of the initiator, the resulting free-volume and the interaction of the chemical blocks with the sulfonic domain.

ACKNOWLEDGMENTS

Financial support from the DOD through grants W911-NF-11-10486 and W911-NF-14–10076(SAXS equipment) is acknowledged. The authors would also like to acknowledge Dr. Roberto Olayo for his insightful suggestion about the polymerization reactions. Finally, the authors would also like to acknowledge Dr. Jeremiah Hubbard and Aracelis Cardona for the help and support with the TGA and NMR experiments, respectively.

REFERENCES

1. Drobny, J. G. Technology of Fluoropolymers, 2nd ed.; CRC Press: Boca Raton, FL, **2008**, pp. 171–179.
2. Peckham, T. J.; Yang, Y.; Holdcroft, S. In Proton Exchange Membrane Fuel Cells. Materials Properties and Performance; Wilkinson, D. P.; Zhang, J.; Fergus, J.; Li, X., Eds.; CRC Press: Boca Raton, FL, **2009**, pp. 108–171.
3. Mady, M. F.; Bak, J. M.; Lee, H.; Kelland, M. A. *Chem. Eng. Sci.* **2014**, *119*, 230.
4. Rao, V.; Friedrich, K. A.; Stimming, U. In Handbook of Membrane Separations. Chemical, Pharmaceutical, Food and Biotechnology Applications; Pabby, A. K.; Rizvi, S. S. H.; Sastre, A. M., Eds.; CRC Press: Boca Raton, FL, **2009**, pp. 760–814.
5. Khapli, S.; Jagannathan, R. J. *Supercrit. Fluids.* **2014**, *85*, 49.
6. Ebnesajjad, S.; Morgan, R. A. In Fluoropolymer Additives; Morgan, S. E. A., Ed.; William Andrew Publishing: Oxford, **2012**; Chapter 6, pp. 69–106.
7. Drobny, J. G. In Technology of Fluoropolymers, 2nd ed.; CRC Press: Boca Raton, FL, **2008**, pp. 29–56.
8. Peighambardoust, S. J.; Rowshanzamir, S.; Amjadi, M. *Int. J. Hydrogen Energy* **2010**, *35*, 9349.
9. Li, L.; Su, L.; Zhang, Y. *Int. J. Hydrogen Energy* **2012**, *37*, 4439.
10. Dutta, K.; Das, S.; Patit Paban Kundu, P. P. *J. Membr. Sci.* **2015**, *473*, 94.
11. Mondal, S.; Soam, S.; Kundu, P. P. *J. Membr. Sci.* **2015**, *474*, 140.
12. Iwai, Y.; Ikemoto, S.; Haramaki, K.; Hattori, R.; Yonezawa, S. *J. Supercrit. Fluids* **2014**, *94*, 48.
13. Sun, L.; Thrasher, J. S. *Polym. Degrad. Stab.* **2005**, *89*, 43.
14. Yang, L.; Tang, B.; Wu, P. *J. Memb. Sci.* **2014**, *467*, 236.
15. Avilés-Barreto, S. L.; Suleiman, D. *J. Appl. Polym. Sci.* **2013**, *129*, 2294.
16. Barreto, S. M. A.; Suleiman, D. *J. Membr. Sci.* **2010**, *362*, 471.

17. Pulido Ayazo, J. C.; Suleiman, D. *J. Appl. Polym. Sci.* **2012**, *124*, 145.
18. Guerrero-Gutiérrez, E. M. A.; Suleiman, D. *J. Appl. Polym. Sci.* **2013**, *129*, 73.
19. Hansen, N. M. L.; Jankova, K.; Hvilsted, S. *Eur. Polym. J.* **2007**, *43*, 255.
20. Braunecker, W. A.; Matyjaszewski, K. *Prog. Polym. Sci.* **2007**, *32*, 93.
21. Tunca, U.; Hizal, G.; Acar, M. H. In Handbook of Vinyl Polymers: Radical Polymerization, Process, and Technology; Mishra, M.; Yagci, Y., Eds.; 2nd ed.; CRC Press: Boca Raton, FL, **2008**, pp. 231–305.
22. Matyjaszewski, K. *Macromolecules* **2012**, *45*, 4015.
23. Hvilsted, S. *Polym. Int.* **2014**, *63*, 814.
24. Becker, M. L.; Remsen, E. E.; Wooley, K. L. *J. Polym. Sci. Part A Polym. Chem.* **2001**, *39*, 4152.
25. Dimitrov, I.; Takamuku, S.; Jankova, K.; Jannasch, P.; Hvilsted, S. *Macromol. Rapid Commun.* **2012**, *33*, 1368.
26. Dimitrov, I.; Takamuku, S.; Jankova, K.; Jannasch, P.; Hvilsted, S. *J. Membr. Sci.* **2014**, *450* 362.
27. Perrier, S.; Jackson, S. G.; Haddleton, D. M.; Ameduri, B. *Tetrahedron* **2002**, *58*, 4053.
28. Shemper, B. S.; Mathias, L. *J. Eur. Polym. J.* **2004**, *40*, 651.
29. Jankova, K.; Chen, X.; Kops, J.; Batsberg, W. *Macromolecules* **1998**, *31*, 538.
30. Howell, B. A.; Johnson, M. J.; Player, D. E.; Hahnfeld, L. J.; Kling, S. M.; Mounts, M. L. *J. Therm. Anal. Calorim.* **2006**, *85*, 209.
31. Jankova, K.; Hvilsted, S. *J. Fluor. Chem.* **2005**, *126*, 241.
32. Jankova, K.; Hvilsted, S. *Macromolecules* **2003**, *36*, 1753.
33. Crank, J. In The Mathematics of Diffusion; Oxford University Press: Oxford, **1975**; Chapter 4, pp 50–51.
34. Elabd, Y. A.; Napadensky, E.; Sloan, J. M.; Crawford, D. M.; Walker, C. W. *J. Membr. Sci.* **2003**, *217*, 227.
35. Zhang, H.; Ma, C.; Wang, J.; Wang, X.; Bai, H. J.; Liu, *Int. J. Hydrogen Energy.* **2014**, *39*, 974.
36. Çekingen, S. K.; Saltan, F.; Yildirim, Y.; Akat, H. *Thermochim. Acta* **2012**, *546*, 87.
37. He, G.; Zhang, G.; Hu, J.; Sun, J.; Hu, S.; Li, Y.; Liu, F.; Xiao, D.; Zou, H.; Liu, G. *J. Fluor. Chem.* **2011**, *132*, 56.
38. Hansen, N. M. L.; Gerstenberg, M.; Haddleton, D. M.; Hvilsted, S. *J. Polym. Sci. Part A Polym. Chem.* **2008**, *46*, 8097.
39. Suleiman, D.; Napadensky, E.; Sloan, J. M.; Crawford, D. M. *Thermochim. Acta* **2007**, *460*, 35.
40. Lampman, G. M.; Pavia, D. L.; Kriz, G. S.; Vyvyan, J. R. Introduction to Spectroscopy, 4th ed.; Brooks/Cole, Cengage Learning: Belmont, CA, **2010**, pp 397–412.
41. Allison, J. P. *J. Polym. Sci. Part A-1 Polym. Chem.* **1966**, *4*, 1209.
42. Zidan, H. M.; El-Khodary, A.; El-Sayed, I. A.; El-Bohy, H. I. *J. Appl. Polym. Sci.* **2010**, *117*, 1416.
43. Rosen, S. Fundamental Principles of Polymeric Materials; SPE Monograph Series; Wiley Interscience Publication: New York, NY, **1993**; p 110.
44. Elabd, Y. A.; Napadensky, E.; Sloan, J. M.; Walker, C. W.; Winey, K. I. *Macromolecules* **2006**, *39*, 399.
45. Moore, H. D.; Saito, T.; Hickner, M. A. *J. Mater. Chem.* **2010**, *20*, 6316.
46. Narsimlu, N.; Siva Kumar, K.; Wu, C.-E.; Wu, C. G. *Mater. Lett.* **2003**, *57*, 2729.
47. Das, S.; Kumar, P.; Dutta, K.; Kundu, P. P. *Appl. Energy* **2014**, *113*, 169.
48. Moukheiber, E.; De Moor, G.; Flandin, L.; Bas, C. *J. Membr. Sci.* **2012**, *389*, 294.
49. Dutta, K.; Das, S.; Kundu, P. P. *J. Membr. Sci.* **2015**, *473*, 94.
50. Wei, Z.; He, S.; Liu, X.; Qiao, J.; Lin, J.; Zhang, L. *Polymer* **2013**, *54*, 1243.
51. Na, T.; Shao, K.; Zhu, J.; Liu, Z. H., ; Sun, H.; Lew, C. M.; Zhang, Z.; Zhang, G. *Polymer* **2012**, *53*, 4413.
52. Na, T.; Shao, K.; Zhu, J.; Sun, H.; Liu, Z.; Zhao, C.; Zhang, Z.; Lew, C. M.; Zhang, G. *J. Membr. Sci.* **2012**, 417, *61*.
53. Kim, E.; Weck, P. F.; Balakrishnan, N.; Bae, C. *J. Phys. Chem. B* **2008**, *112*, 3283.
54. Avilés-Barreto, S. L.; Suleiman, D. *J. Membr. Sci.* **2015**, *474*, 92.
55. Budd, P. M.; McKeown, N. B.; Fritsch, D. J. *Mater. Chem.* **2005**, *15*, 1977.